

Structural Constraints Imposed by the Conserved Fusion Peptide on the HIV-1 gp41 Epitope Recognized by the Broadly Neutralizing Antibody 2F5[†]

Igor de la Arada,[‡] Jean-Philippe Julien,[§] Beatriz G. de la Torre,^{||} Nerea Huarte,[‡] David Andreu,^{||} Emil F. Pai,^{§,†,#} José L. R. Arrondo,[‡] and José L. Nieva*,[‡]

Biophysics Unit (CSIC-UPV/EHU) and Department of Biochemistry and Molecular Biology, University of the Basque Country, P.O. Box 644, 48080 Bilbao, Spain, Departments of Biochemistry and Medical Biophysics and Molecular Genetics, University of Toronto, 1 King's College Circle, Toronto, Ontario, Canada M5S 1A8, Division of Cancer Genomics and Proteomics, Ontario Cancer Institute, MaRS/TMDT, 101 College Street, Toronto, Ontario, Canada M5G 1L7, and Proteomics Unit, Pompeu Fabra University, Dr. Aiguader 80, 08003 Barcelona, Spain

Received: June 25, 2009; Revised Manuscript Received: August 6, 2009

The HIV-1 gp41 epitope recognized by the broadly neutralizing 2F5 antibody has focused much attention as a suitable target in the design of peptide immunogens. Peptides mimicking the linear 2F5 epitope (2F5ep) are however intrinsically disordered, while the structural constraints existing in the cognate gp41 native structure recognized by the antibody are presently unknown. In recent reports, we have shown that core residues of the amino-terminal fusion peptide (FP) increase MAbs2F5 affinity. Here, we have inferred the sequence-specific structural constraints imposed by the FP residues on the 2F5 epitope from the comparison of two hybrid peptides: HybK3, which connects through a flexible tether residues derived from 2F5ep and FP sequences, and scrHybK3, combining 2F5ep and an FP sequence with the conserved core scrambled. Circular dichroism, conventional and two-dimensional correlation infrared spectroscopy, and X-ray diffraction studies revealed specific structural features that were dependent on the exact FP sequence, namely, (i) the production with moderate low polarity of an intermediate folded structure enriched in β -turns and α -helix; (ii) the existence in this intermediate of a thermotropic conformational transition taking place at ca. 18–20 °C, consistent with the conversion of 3_{10} -helices into β -turn conformers; and (iii) the presence of a C-terminal α -helix in crystals of Fab'–peptide complexes. Those features support the existence of native-like tertiary interactions between FP and 2F5 epitope residues, which might be important to recreate when developing an effective AIDS peptide vaccine.

Introduction

The generation of an immunogen capable of eliciting broadly neutralizing antibodies (bNAbs) to human immunodeficiency virus type 1 (HIV-1) constitutes a challenging task in the development of a potentially protective AIDS vaccine.^{1–3} bNAbs are rarely induced through immunization because of the structural adaptations present in their main targets, the virion envelope glycoproteins (Env) gp120 and gp41 that mediate receptor binding and cell entry.^{2,4} Nonetheless, a few effective anti-HIV-1 bNAbs have been recovered from chronically infected individuals in the form of monoclonal antibodies (mAb-s), thereby suggesting that bNAbs production through immunization can be an attainable goal.^{1,3–5} It has been proposed that potential immunogens could be designed on the basis of the molecular structures recognized by these mAb-s on the Env antigen surface.⁶ It is predicted that a

formulation mimicking the epitope structure recognized by a particular NAb would elicit neutralizing immune responses with the same and almost unique specificity. MAbs2F5, the object of the present study, simultaneously exerts broad and potent neutralizing activity across different HIV-1 strains and isolates *in vitro*,^{7,8} interrupts mucosal transmission and viral spread,⁹ and confers protection to viral infection when passively transferred to primate models.^{10,11} The bNAbs 2F5 recognizes a linear epitope located within the “membrane-proximal external region” (MPER) domain of the transmembrane gp41 subunit (Figure 1A). MPER is functional in fusion and highly conserved across viral clades, and consequently constitutes a suitable target for peptide-based vaccine development.^{12,13} However, attempts to generate bNAbs with 2F5 specificity using peptide epitopes as immunogens have failed so far.^{1,4} The existence of an unidentified factor that confers immunogenicity to the 2F5 epitope in the native prefusion state of gp41 has been invoked to explain this lack of success.¹

Atomic structures of prefusion versions of the gp41 ectodomain including the 2F5 epitope region are not presently available. However, the native-like structures recognized by MAbs2F5 can be inferred from crystal structures of the antigen-binding fragment (2F5 Fab') complexed with peptide epitopes. Initial X-ray diffraction studies revealed that the core 662ELDK-WAS668 epitope (numbering based on prototypic HXBc2 isolate) adopts a closed, slightly distorted, type I β -turn

* To whom correspondence should be addressed. Phone: +34 94 601 3353. Fax: +34 94 601 3360. E-mail: gbpniej@lg.ehu.es.

[†] University of the Basque Country.

[§] Department of Biochemistry, University of Toronto.

^{||} Pompeu Fabra University.

[#] Department of Medical Biophysics and Molecular Genetics, University of Toronto.

[#] Ontario Cancer Institute.

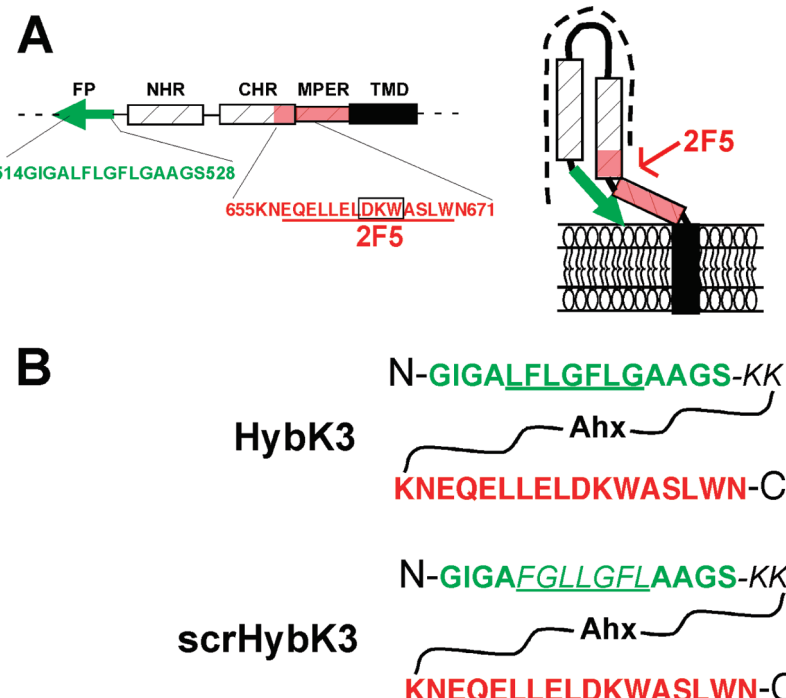


Figure 1. Design of FP–2F5 epitope hybrid sequences. (A) Left: Schematic gp41 diagram disclosing the different functional regions: FP, fusion peptide; NHR and CHR, amino- and carboxy-terminal helical regions, respectively; MPER, membrane-proximal external region; TMD, transmembrane domain. The FP and 2F5 epitope sequences selected to construct the hybrids span the 514–528 (green) and 655–671 (red) regions, respectively (Env sequences and numbering derived from the prototypic HXBc2 isolate). The 2F5 epitope sequence in the box designates turn core residues crucial for antibody recognition. Right: Model of a gp41 monomer anchored to the viral membrane highlighting the possibility that FP and MPER residues establish contacts in the vicinity of the membrane interface. The dotted line indicates the putative surface covered by quaternary contacts.⁵² (B) The hybrid sequences used in this study connect amino-terminal FP (514–528) and 2F5 epitope (655–671) residues (green and red sequences, respectively) through a flexible amino hexanoic acid (Ahx) spacer. In addition, the conserved 518LFLGFLG524 FP motif³⁰ (underlined) has been scrambled to produce scrHybK3 (underlined and italics).

conformation.¹⁴ This core structure was retained in peptide epitopes elongated to increase antibody affinity.^{15,16} On the basis of the prediction that the N- and C-terminal ends of the gp41 ectodomain may be found in close proximity in a prefusion state, we proposed that contacts between the gp41 conserved FP and 2F5ep regions may stabilize an immunogenic stem-like tertiary complex.^{17,18} Supporting the proposal that 2F5 constitutes a conformational antigenic determinant, X-ray diffraction data from a 2F5 Fab'–peptide complex crystal revealed that the core β -turn motif was followed by the initiation of a canonical α -helix in the presence of FP residues.¹⁶

Here, we have analyzed the FP-imposed structural constraints on the 2F5 epitope using a hybrid sequence, HybK3, that connected through a flexible tether residues derived from both gp41 domains (Figure 1B). The relevance of the observed effects has been contrasted by inducing unspecific hydrophobic interactions within scrHybK3, a control peptide with identical composition but with the conserved FP heptad scrambled (Figure 1B). HybK3 and scrHybK3 structures were compared by circular dichroism (CD) and infrared spectroscopy (IR) as a function of medium polarity and temperature, two factors predicted to modulate 2F5 epitope native conformation.^{15,19–21} With moderate low polarity, the native-like FP–2F5ep hybrid sequence folded into an intermediate structure enriched in β -turn and α -helix conformers. In contrast, under the same experimental conditions, scrHybK3 folded into a structure enriched in extended and β -turn conformers that also showed features of denaturation. The conventional and two-dimensional correlation IR spectroscopy (2D-COS) study of the thermal behavior of these hybrids revealed a conformational transition at ca. 18–20 °C for HybK3, consistent with the conversion of 3_{10} -helices into β -turns, which

was not observed for scrHybK3. Specifically, 3_{10} -helix and α -helix conformers populated the HybK3 structure at low temperatures and also in the lowest polarity media, and β -turn and α -helices above the transition temperature, under moderate low polarity conditions.

In agreement with the spectroscopy data, X-ray diffraction studies on 2F5 Fab'–peptide complexes revealed that HybK3 and scrHybK3 carboxy termini, respectively, adopted β -turn + α -helix and β -turn + disordered structures in contact with the paratope. These findings suggest that folding of the 2F5 epitope carboxy-terminus as an α -helix was dependent on the presence of FP residues in the correct order. We discuss the importance that recreating FP-induced constraints in secondary structure might have for the production of native-like gp41 2F5 epitope in a peptide vaccine formulation.

Experimental Methods

Materials. The HybK3 and scrHybK3 peptides (sequences displayed in Figure 1) were synthesized in C-terminal carboxamide form by solid-phase methods using Fmoc chemistry, purified by reverse phase HPLC, and characterized by matrix-assisted time-of-flight (MALDI-TOF) mass spectrometry (purity >95%). Peptides were dissolved in dimethylsulfoxide (DMSO, spectroscopy grade) and their concentration determined by the bicinchoninic acid microassay (Pierce, Rockford, IL). Preparation of the 2F5 Fab' fragment by enzymatic digestion of the full IgG was previously described.²²

Circular Dichroism. Circular dichroism (CD) measurements were carried out on a thermally controlled Jasco J-810 circular dichroism spectropolarimeter calibrated routinely with (1*S*)-(+)–

10-camphorsulfonic acid, ammonium salt. Stock samples consisted of peptide dissolved in DMSO, lyophilized and finally dissolved in 2 mM Hepes (pH 7.4) at 0.03 mM concentration. Spectra were measured in a 1 mm path-length quartz cell initially equilibrated at 25 °C. Data were taken with a 1 nm bandwidth, 100 nm/min speed, and the results of 20 scans were averaged.

Infrared Spectroscopy. Infrared spectra were recorded in a Bruker Tensor 27 spectrometer equipped with a mercury–cadmium–telluride detector using a Peltier-based temperature controller (TempCon, BioTools Inc., Wauconda, IL) with calcium fluoride cells (BioCell, BioTools Inc., Wauconda, IL). HybK3 and scrHybK3 peptides were lyophilized and subsequently prepared at 4 mg/mL in D₂O buffer (5 mM Hepes pH 7.4, 100 mM NaCl). A 25 μL sample aliquot was deposited on a cell that was sealed with a second cell. Reference windows without peptide were prepared similarly. Typically, 1000 scans were collected for each background and sample, and the spectra were obtained with a nominal resolution of 2 cm⁻¹. Data treatment and band decomposition of the original amide I have been described elsewhere.²³ To obtain the 2D-IR maps, temperature was used to induce spectral fluctuations and to detect dynamic spectral variation in the secondary structure of HybK3 and scrHybK3. Spectra were collected in the 4–50 °C interval in 1° steps. Rendering of the two-dimensional synchronous and asynchronous spectra has been described previously.²⁴

X-ray Crystallography. The crystal structure of 2F5 Fab' in complex with peptide HybK3 (PDB ID: 3D0L) was reported elsewhere.¹⁶ To obtain crystals of the 2F5 Fab' in complex with the scrHybK3 construct, the lyophilized peptide was dissolved in DMSO and mixed with the 2F5 Fab' in a molar ratio of peptide to protein of 10:1. Crystals were grown using the hanging drop vapor diffusion method with the 2F5 Fab' concentration at 9 mg/mL in a solution containing 20 mM Tris/HCl, pH 8.0, 0.1% Tween-20. The volume of the drops was 2 μL, with a 1:1 mix of protein solution and reservoir solution. Crystals were obtained above a reservoir solution containing 0.1 M sodium acetate, pH 5.6, 16% 2-propanol, and 16% PEG 4000 (PDB ID: 3DRT). All crystallization experiments were carried out at room temperature. In order to reproduce the environment in which cocrystals of 2F5 Fab'-HybK3 were obtained,¹⁶ some of the 2F5 Fab'-scrHybK3 cocrystals were soaked in 1.6 M ammonium sulfate solution (PDB ID: 3EGS). Before being flash-frozen in a stream of boiling nitrogen, crystals were soaked for a few seconds in reservoir solution supplemented with 15–20% glycerol. The 2F5 Fab'-scrHybK3 crystals were thin needles, brittle in nature, difficult to handle and to reproduce, as well as very short-lived when exposed to a strong X-ray beam. For this reason, X-ray diffraction data were collected on a home source, a Rigaku MicroMax-007 HF at 40 kV and 30 mA with Osmic multilayer optics and a Mar345 image plate detector. Raw diffraction data were reduced using the program XDS.²⁵

The maximum resolutions obtained for the native and soaked crystals were 3.3 and 3.6 Å, respectively. In addition, the low $I/\sigma(I)$ resulted in overall poor statistics for the diffraction data (refer to Table 3 for complete crystallographic statistics). To confirm that these diffraction data could be used to detect differences in the secondary structure of the bound peptide epitopes, we performed the following checks. First, we made sure that the crystal was not twinned by probing the data set with the Padilla–Yeates algorithm (<http://nihserver.mbi.ucla.edu/pystats/>). Subsequently, we confirmed that the 2F5 Fab'-scrHybK3 crystals obtained were isomorphous with 2F5

Fab' complex crystals previously analyzed using higher resolution data. The crystals could be phased directly from a well-refined, high resolution model (PDB ID: 3D0L). Refinement was then started in CNS²⁶ by directly placing the model into the rigid-body cycle. Interpretation of electron density was done with the help of the program Coot.²⁷ Comparison of the two 2F5 Fab'-scrHybK3 models with previously published 2F5 Fab' crystal complexes showed rmsd values for all C_α atoms smaller than 0.2 Å, and rmsd values ranging from 0.2 to 0.6 Å for all atoms, confirming the close structural similarity between starting model and final model, i.e., the good quality of the phases underlying the electron density calculations. Both structures refined to R_{crys} and R_{frees} in the low 20s (Table 3). Analysis of contact surface areas between residues of the epitope and the antibody fragment was performed using the program ICM.²⁸

Results

The HIV-1 gp41 schematic diagrams displayed in Figure 1A illustrate the rationale underlying the design of the hybrid peptides used in this study. According to our hypothesis, the N-terminal FP and the MPER 2F5 epitope sequence might assemble into a complex in a gp41 prefusion state. This complex would locate in close proximity of the water–membrane interface and therefore be affected by the reduction in medium polarity.²⁹ Moreover, it has been shown that Env expressing cells expose 2F5 epitope only above 19 °C, reflecting the existence of temperature-dependent conformational elements on the prefusion native antigen.²¹

The HybK3 peptide's sequence displayed in Figure 1B combined FP core residues with the 2F5ep. It also incorporated three Lys residues, one of which corresponds to the Lys655 preceding the 2F5 epitope in HIV-1 Env, that were added to increase the construct's solubility.¹⁸ In the scrHybK3 sequence, the FP conserved motif (underlined)³⁰ was scrambled with the aim of inducing unspecific hydrophobic interactions between both domains. Given the fact that 2F5 epitope structure and dynamics are likely to be conditioned by changes in polarity occurring in short range at the membrane interface and by temperature, the structures of the hybrid peptides were compared as a function of these two factors.

Effect of Medium Polarity and Temperature on FP–2F5ep Hybrid Structure. The structural characterization displayed in Figure 2 supports that FP residues in a correct order stabilize a β-turn/α-helix conformation in mildly nonpolar conditions mimicking the membrane interface region. The CD spectrum of HybK3 in buffer indicated a low level of structuring and features of certain β-rich proteins (Figure 2A, left top panel).³¹ Consistently, IR spectra obtained in D₂O buffer for HybK3 displayed main absorption at 1642 and 1623 cm⁻¹, two bands that can be assigned to unordered structures and aggregation/denaturation, respectively (Figure 2A, right top panel).^{23,32} In contrast, the scrHybK3 CD spectrum displayed absorption minima at 206 and 221 nm. It has been proposed that conformers containing a considerable population of type I β-turns could give rise to similar CD spectra.³³ Consistent with this idea, the main feature of the amide I region of the corresponding scrHybK3 IR spectrum was a band centered at 1673 cm⁻¹.^{23,32} In addition, the scrHybK3 spectrum displayed absorption maxima at 1655 and 1623 cm⁻¹, arising from helical conformers and aggregation/denaturation, respectively. In summary, HybK3, the construct containing FP residues in the correct order, remained overall unstructured in buffer solution, while the induction of unspecific hydrophobic interactions within the

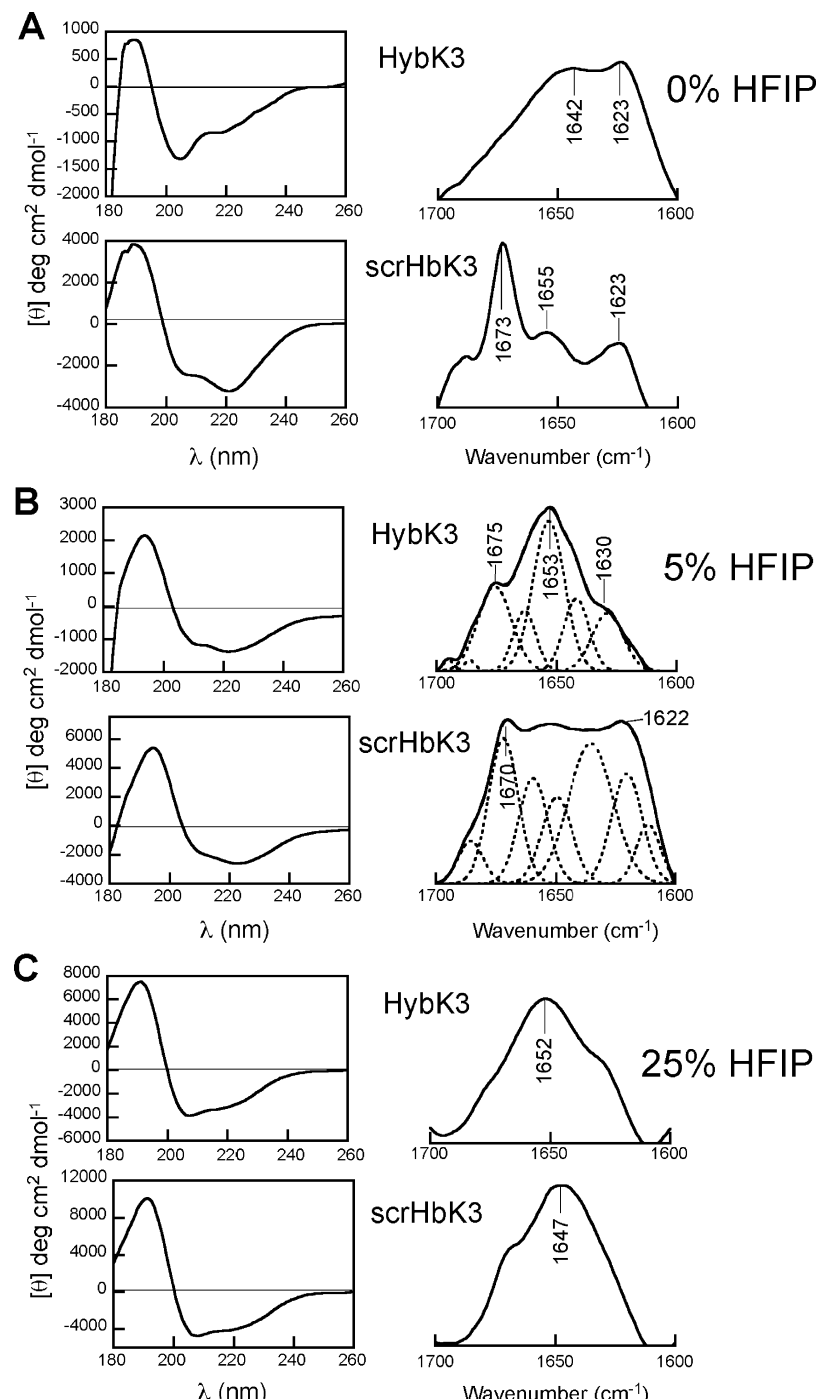


Figure 2. Structural analysis of HybK3⁵¹⁴GIGALFLGFLGAAGS⁵²⁸KK-Ahx⁶⁵⁵KNEQELLELDKWASLWN⁶⁷¹ and scrHybK3⁵¹⁴GIGAFGLLGFLAAGS⁵²⁸KK-Ahx⁶⁵⁵KNEQELLELDKWASLWN⁶⁷¹ (top and bottom panels, respectively). CD (left panels) and IR (right panels) spectra were obtained at 25 °C in media containing increasing amounts of 1,1,1,3,3-hexafluoro-2-propanol (HFIP). (A) Samples in buffer. (B) Samples in buffer containing 5% HFIP (v/v). The amide I regions of these IR spectra were decomposed (dotted lines correspond to the different band components). The original spectrum and the sum of the band components are superimposed and indistinguishable. The numerical values are presented in Table 1. (C) Samples in buffer containing 25% HFIP (v/v).

scrHybK3 sequence seemed to stabilize mainly β -turns in an overall aggregated/denatured structure.

A subtle reduction in the medium polarity induced important structural rearrangements in HybK3 (Figure 2B). The CD spectrum in a medium containing 5% 1,1,1,3,3-hexafluoro-2-propanol (HFIP) displayed a negative peak at ca. 210 nm together with stronger absorption centered at 222 nm, which suggested the existence of helix–helix interactions^{34,35} and/or an enrichment in type I β -turn conformers³³ in these samples (Figure 2B, left top panel). The amide I region of the

corresponding IR spectra denoted prominent bands centered at 1675 and 1653 cm^{-1} (Figure 2B, right top panel), confirming β -turn and α -helix, respectively, as the main conformations adopted by this peptide in 5% HFIP. A shoulder centered at 1630 cm^{-1} indicated an additional contribution of β -sheet conformation, while no bands arising from aggregation/denaturation could be observed in these samples. Structural changes induced by the reduction in the medium polarity were not so evident from the scrHybK3 CD spectrum. By comparison, broadening of the amide I IR band denoted an increase in

TABLE 1: Band Position, Assignment, and % Area of the Components Obtained after Curve-Fitting of IR Spectra Displayed in Figure 2B

HybK3		ScrHybK3	
band position ^a	area ^b (%)	band position ^a	area ^b (%)
1675 (β -turns)	23	1672 (β -turns)	19
1663 (β -helix)	10	1660 (β -helix)	14
1653 (α -helix)	37	1650 (α -helix)	12
1642 (unordered)	14	1635 (unordered/ β -sheet)	28
1630 (β -sheet)	14	1611/1620/1686 (aggregation)	26

^a Wavenumbers in cm^{-1} . The conformation assigned for each position²³ is indicated below. ^b The values have been rounded off to the nearest integer.

scrHybK3 disorder with lower polarity (see below). Nonetheless, absorption peaks located at 1670 and 1622 cm^{-1} indicated that β -turn and aggregation/denaturation still contributed importantly to the scrHybK3 structure under these conditions.

Decreasing further the medium polarity induced comparable effects on HybK3 and scrHybK3 CD spectra, which displayed in 25% HFIP features of the main helix conformation, namely, minima at 208 and shoulders at ca. 222 nm (Figure 2C, left panels). The corresponding IR spectra also showed mean features of helical conformation. The scrHybK3 absorption maximum shifted to 1647 cm^{-1} , however suggested the presence of helical conformers more exposed to solvent and/or a higher degree of disorder in this case.³²

Thus, the combined CD and IR structural analysis as a function of the decreasing medium polarity revealed the presence of a HybK3 folded intermediate between unordered and helical structures. Band decomposition of this intermediate amide I band (Figure 2B, right top panel and Table 1) confirmed main contributions of 1675 cm^{-1} (β -turns) and 1653 cm^{-1} (α -helix) to the overall absorption (in combination, approximately 60% of the total band area). Contribution of absorption centered at 1642 and 1630 cm^{-1} was indicative of an additional fraction of unordered (14%) and β -type extended structures (14%). By comparison, the main features of scrHybK3 spectra (Figure 2B, right bottom panel and Table 1) included a prominent band centered at $\approx 1635 \text{ cm}^{-1}$ (unordered + extended structures) and aggregation bands at 1611, 1620, and 1685 cm^{-1} (54% of the total band area in combination), which evidenced a high degree of unstructuring/denaturation for this sequence. Moreover, the band attributable to α -helix (centered at $\approx 1650 \text{ cm}^{-1}$) did not contribute significantly to the overall spectrum (12% of the total area), which still disclosed a significant contribution of the 1672 cm^{-1} band (β -turns, 19% of the area).

Thus, the quantitative IR analysis above suggests that the correct FP sequence is required for the induction of significant α -helix content, as well as for the proper folding of the hybrid sequence in a moderate low polarity medium. Scrambling the FP core sequence resulted in low α -helix content and an overall destabilization of this structure. The results displayed in Figures 3–6 and Table 2 further support a dependence of the HybK3 folded structure on medium polarity and temperature. IR spectra displayed in Figure 3 correspond to samples measured with various HFIP contents, and they were obtained at three different temperatures, 4, 20, and 50 °C. The spectra of the HybK3 samples measured at 4 °C showed a component centered at

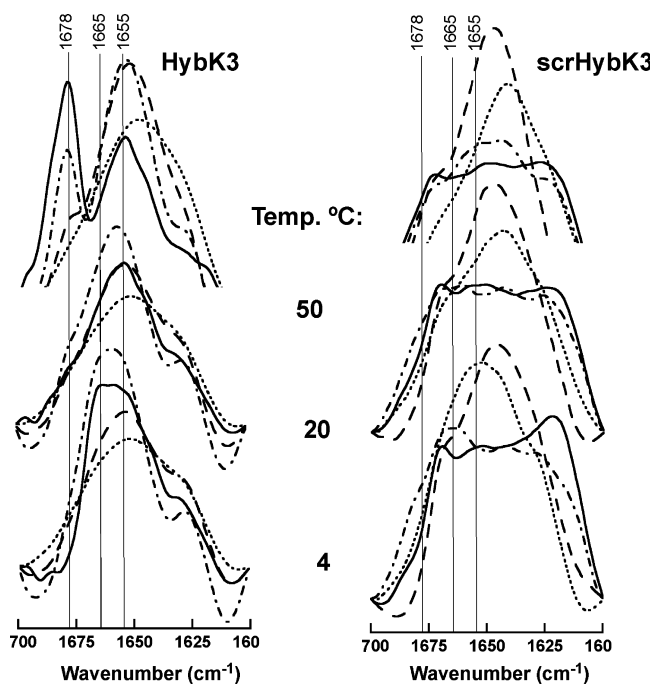


Figure 3. Amide I region IR spectra of HybK3 and scrHybK3 measured in D_2O -based buffer with various amounts of HFIP were obtained at 4, 20, and 50 °C (bottom, middle, and top spectra, respectively). HFIP percentages (v/v): 5% (continuous), 12.5% (dotted-slash), 25% (slashed), and 50% (dotted).

$\approx 1665 \text{ cm}^{-1}$ in 5 and 12.5% HFIP. Decreasing the polarity of the medium reduced this band's contribution and a concomitant increase of the absorption centered at 1655 cm^{-1} . Conversely, the 50 °C samples showed a predominant band centered at $\approx 1678 \text{ cm}^{-1}$ in 5 and 12.5% HFIP, which was absent from the amide I contour at 4 °C. Moreover, these spectra did not show any discernible peak at 1665 cm^{-1} . Again, a decrease in medium polarity induced the disappearance of the 1678 cm^{-1} band, and a relative increase in the absorption centered at 1655 cm^{-1} . The 20 °C spectra represented intermediate states in which bands centered at 1655 cm^{-1} were predominantly visible.

These temperature-driven changes were not observed in the corresponding scrHybK3 spectra, which invariably showed an apparent 1678–1675 cm^{-1} band at all temperatures in 5 and 12.5% HFIP samples. The higher HFIP content also reduced the contribution of the 1678–1675 cm^{-1} band in these samples. Interestingly however, bands centered at $\approx 1645 \text{ cm}^{-1}$, which are assigned to unordered structures, became dominant in the scrHybK3 spectra recorded with decreasing polarity. Thus, in addition to abolishing the temperature effect on the 1678–1665 cm^{-1} region, it seems that scrambling the conserved FP residues also altered the conformations accessible to HybK3 in the low polarity medium.

Thermotropic Conformational Transition in FP-2F5ep Hybrids. The effect of temperature on hybrid folded structure was subsequently characterized in samples subjected to a heating cycle. Figure 4A (top panel) shows the conformational transition undergone by the HybK3 5% HFIP sample as evidenced from the thermal profile of the amide I band in the 4–50 °C interval. A transition was apparent at $\approx 20 \text{ }^\circ\text{C}$ as an increase in the 1678 cm^{-1} peak, while the one centered at 1666 cm^{-1} decreased. The transition was abolished either by scrambling the FP sequence (scrHybK3 5% HFIP) or by decreasing medium polarity (HybK3 50% HFIP) (center and bottom panels in Figure 4A, respectively). Thus, the species

TABLE 2: Band Position, Assignment, and % Area of the Components Obtained after Curve-Fitting of HybK3 IR Spectra Displayed in Figure 8A

5% HFIP				50% HFIP			
4 °C		50 °C		4 °C		50 °C	
band position ^a	area ^b (%)	band position ^a	area ^b (%)	band position ^a	area ^b (%)	band position ^a	area ^b (%)
1678 (β -turns)	0	1677 (β -turns)	37	1679 (β -turns)	8	1679 (β -turns)	6
1667 (3_{10} -helix)	26	1663 (3_{10} -helix)	6.5	1667 (3_{10} -helix)	20	1665 (3_{10} -helix)	19
1654 (α -helix)	47	1654 (α -helix)	30	1654 (α -helix)	30	1652 (α -helix)	29
1642 (unordered)	11	1643 (unordered)	11	1642 (unordered)	19	1639 (unordered)	25
1630 (β -sheet)	16	1630 (β -sheet)	14.5	1629 (β -sheet)	22	1627 (β -sheet/aggregation)	21

^a Wavenumbers in cm^{-1} . The conformation assigned for each position²³ is indicated below. Intermolecular aggregation bands at ca. 1687 and 1618 cm^{-1} have been omitted from the calculations. ^b The values have been rounded off to the nearest integer.

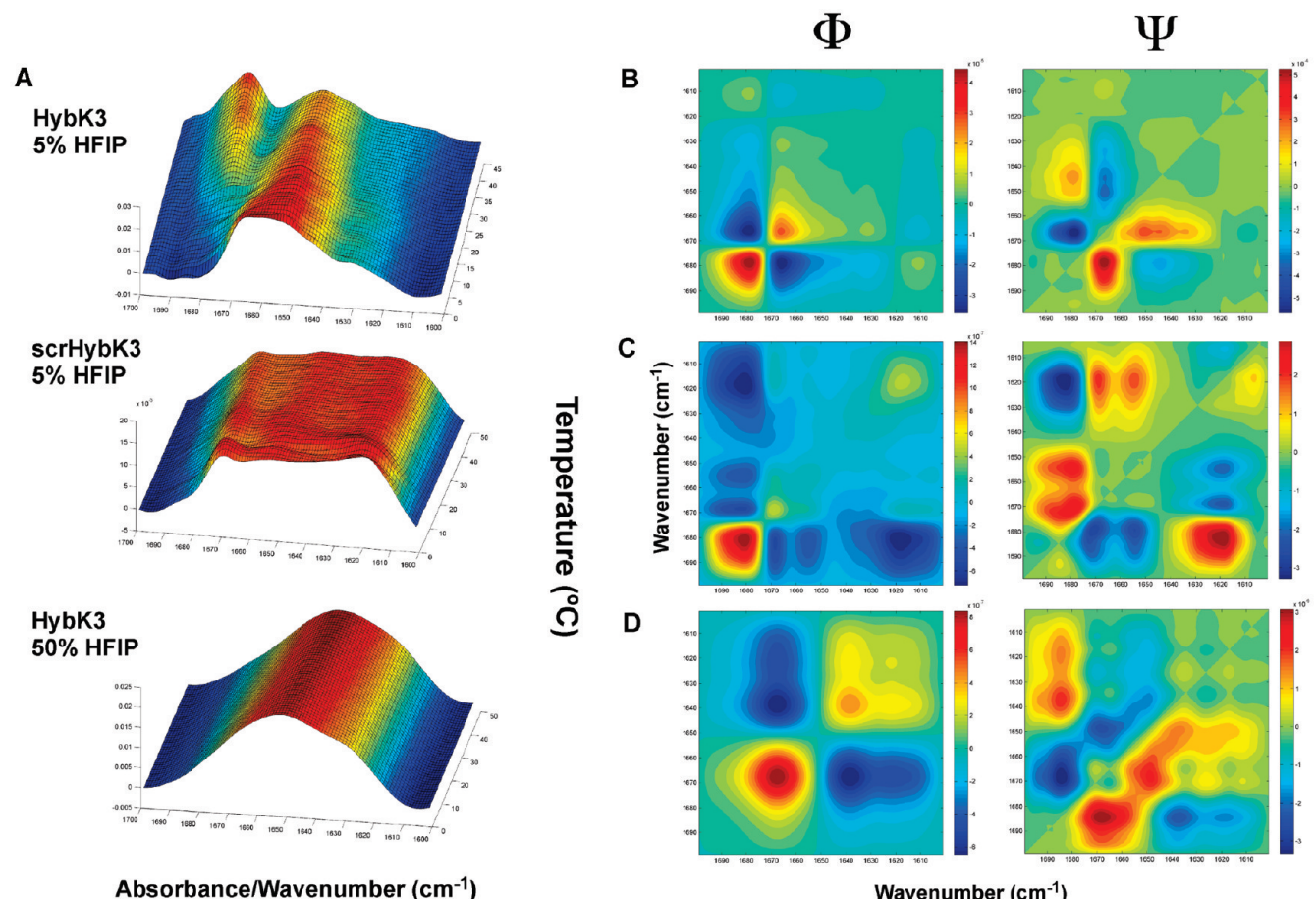


Figure 4. Thermotropic conformational transition in HybK3. (A) Temperature plots of the amide I region in the 4–50 °C interval. The plot for the HybK3 with 5% HFIP shows the appearance of the 1678 cm^{-1} band above ca. 20 °C (top panel). This effect is not observed in the scrHybK3 with 5% HFIP or HybK3 with 50% HFIP samples (center and bottom panels, respectively). (B) 2D-COS IR analysis of the temperature-driven structural transition in the HybK3 5% HFIP sample. Synchronous (left) and asynchronous (right) correlation map contour of the IR spectra for the 4–50 °C interval are shown. Red peaks correspond to positive correlations and blue peaks to negative ones. (C, D) Idem for the scrHybK3 5% HFIP and HybK3 50% HFIP control samples, respectively.

bearing the correct FP sequence underwent a thermal transition that was absent in a peptide of the same composition but with scrambled FP residues.

The specific changes pertaining to this transition were subsequently inferred from the 2D-COS analysis of the spectra (Figure 4B–D). In the synchronous 2D maps (Φ , left panels), the peaks located along the diagonal (autopeaks) corresponded to simultaneous spectral changes induced by temperature.^{24,36,37}

The 2D-COS synchronous plot for the HybK3 5% HFIP sample (panel B, left) showed two main autopeaks at ca. 1678 and 1665 cm^{-1} , indicating that β -turns and 3_{10} -helices, respectively, were the main structures affected by the change in temperature within this interval (see also Table 2). The cross-relation (nondiagonal) peaks indicated two vibrations that were affected in-phase. A negative cross-correlation peak was found for the 1665/1678 cm^{-1} band pair, consistent with the peak intensities displaying

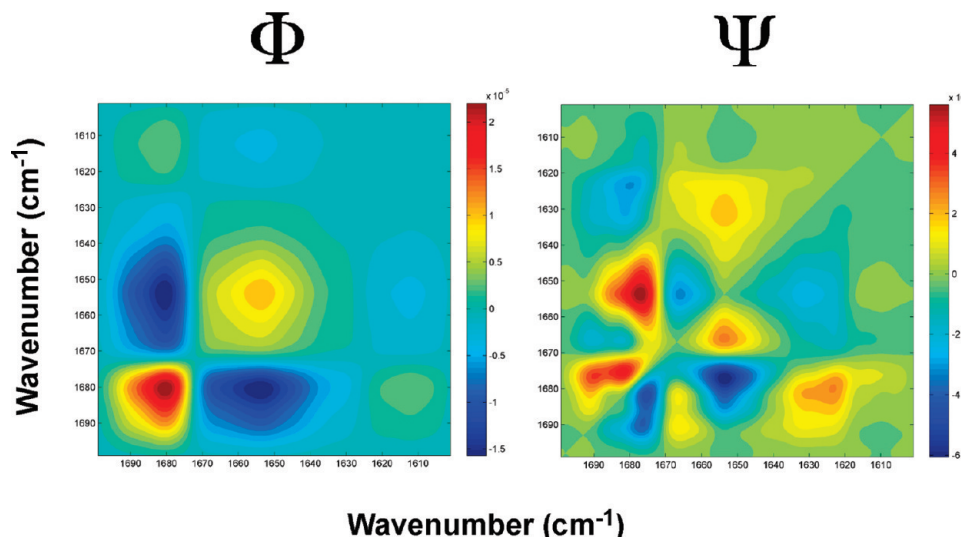


Figure 5. 2D-COS IR analysis of temperature-induced effects on the HybK3 HFIP 5% sample. Maps similar to those displayed in the previous Figure 4B were produced for the 30–80 °C interval.

a contrasting behavior upon the change of temperature (i.e., 1678 cm^{-1} increases whereas 1665 cm^{-1} decreases, panel A).

The corresponding asynchronous map (Ψ , right) showed the not-in-phase cross-relation between the bands and reflected the sequential order of events induced by temperature.^{24,36,37} The asynchronous peak was positive if the change in ν_1 occurred accelerated with respect to that in ν_2 and negative if delayed. The asynchronous plot showed a prominent negative correlation peak for the pair 1665/1678 cm^{-1} . Since the 1665/1678 cm^{-1} region in the synchronous map was also negative, the presence of this peak suggests that temperature-induced changes in 3_{10} -helices preceded those in β -turns. The plot revealed additional cross-peaks, positively correlated as follows: 1645/1678 and 1665/1650. The presence of the first pair indicates that the formation of β -turns may be preceded by a certain amount of more solvated or unordered structures. Absorption within this amide I region has been actually documented for model peptides containing β -turn structure.³⁸ The last pair is consistent with a certain amount of 3_{10} -helices being also converted into α -helices upon heating.

By comparison, the synchronous scrHybK3 map (panel C, left) revealed two main autopeaks at ca. 1685 and 1620 cm^{-1} , consistent with unspecific aggregation being affected by heating, while the corresponding asynchronous map (panel C, right) cross-related these bands and those assigned to canonical structures β -turns (1672 cm^{-1}), 3_{10} helices (1665 cm^{-1}), and α -helices (1655 cm^{-1}). Nonetheless, these effects on the 2D maps involved just subtle changes in the relative contents of the amide I band components (panel A). Also, the amide I band contour of HybK3 HFIP 50% samples showed minor changes upon heating (panel A). The 2D synchronous map for these samples (panel D, right) displayed 1665 and 1640 cm^{-1} autopeaks, which were negatively cross-related, suggesting that 3_{10} -helices were the most sensitive structures to temperature-induced disorder. Again, the absence of defined peaks in the corresponding asynchronous map (panel D, left) further confirms that the thermal treatment induced just minor structural changes, and that such alterations affected simultaneously all amide I band components.

In conclusion, the IR results displayed in Figure 4 support that, within the folded structure produced at moderate low polarity, distinct 3_{10} -helix and nonhelical β -turn structures predominate in HybK3 samples below and above the transition

temperature, respectively, and that these structures interconvert upon heating. While heating induced a conversion of structural components in the former samples, in the scrHybK3 5% HFIP or HybK3 50% HIFP control samples, the same process resulted in changes related to aggregation or disorder.

The effect of temperature on the dynamic β -turn conformation was further evaluated in HybK3 HFIP 5% samples heated from 30 to 80 °C (Figure 5). The synchronous map for this interval (left panel) revealed autopeaks located at 1678 and 1655 cm^{-1} , indicating concomitant changes occurring in the β -turn and α -helical structures, respectively. The negative cross-correlation peak for the 1655/1678 cm^{-1} band pair indicated a decrease of α -helical structure relative to the β -turns that accumulated within this temperature interval. The order of events in the temperature-induced process can be deduced from the asynchronous plot (right panel). Positive correlation for the 1678/1655 cm^{-1} band pair was consistent with changes delayed in α -helices with respect to β -turns. Moreover, the presence of 1678/1623 and 1678/1690 cm^{-1} band pairs suggests that changes in β -turns also preceded the appearance of aggregation-denaturation bands induced by heating. The positively correlated 1665/1655 band pair further indicated that changes in α -helices were also preceded by those in 3_{10} -helices. Thus, β -turns accumulated mainly at the expense of 3_{10} -helices also in this temperature interval. On the other hand, the decrease in α -helix content was most likely related to an increase in disorder and aggregation, as it is also evidenced from the positive correlation broad peak centered at the 1630/1655 cm^{-1} coordinates.

The stability of 3_{10} -helices and β -turns was finally analyzed in samples heated to 90 °C and subsequently subjected to a cooling cycle (heating and cooling proceeding at the same rate of 1 °C/min). Figure 6 displays the spectra obtained at 50, 20, and 4 °C upon cooling the preheated sample. Despite the fact that these IR spectra reflected the appearance of two peaks around 1620 and 1688 cm^{-1} , consistent with the occurrence of peptide aggregation-denaturation, they also revealed the 1678 cm^{-1} (*) and 1665 cm^{-1} (**) peaks present in 50 and 4 °C samples, respectively. Again, the 20 °C sample seemed to consist of an intermediate state in which none of these bands visibly contributed to the IR spectrum contour. Thus, these data support the existence of two stable, essentially different ensembles of HybK3 conformations: one with a high contribution of 3_{10} -helix

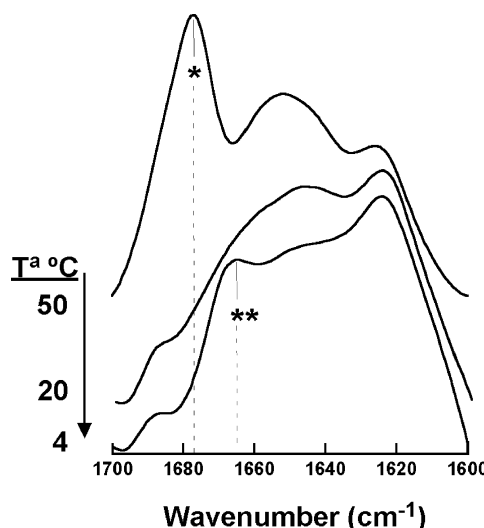


Figure 6. Thermal transition of HybK3 with 5% HFIP observed upon cooling. IR spectra were measured at 50, 20, and 4 °C (top, middle, and bottom spectra, respectively) upon cooling a sample heated to 90 °C (cooling rate, 1 °C/min).

conformer, which exists below ca. 20 °C, and another one, produced above that temperature, which is highly populated by β -turns.

FP Effect on Fab'-Bound 2F5 Epitope Structure. The spectroscopic data above indicated important effects on FP-2F5ep hybrid structure induced by scrambling the core FP residues. FP residues in the correct order essentially stabilized a structural intermediate enriched in β -turn and α -helical structures (Table 1). Scrambling the core FP residues led to denaturation of such structure with a concomitant reduction of the helical conformation. Consistent with those findings, a specific effect of the FP conserved motif can also be observed in the crystal structures of the complexes of 2F5 Fab' with HybK3 (Figure 7A, PDB ID: 3D0L) and scrHybK3 (Figure 7B and C, PDB ID: 3DRT and 3EGS, respectively). As displayed in Figure 7, despite the low resolution (Table 3), the observable electron density is well-defined for both components of the complex, the peptide and the Fab'. Thus, the calculated electron density maps allowed for the clear determination of the presence or absence of ordered secondary structure in the peptide epitopes.

Electron density maps did not reveal the positions of any of the hybrid Gly514-Ser528 FP residues. However, the interpretable electron density spanning the Leu661-Trp670 stretch confirmed the existence of striking differences between the HybK3 and scrHybK3 structures. In the HybK3 structure, amino acids Trp666-Ala667-Ser668-Leu669-Trp670, following the type I β -turn Asp664-Lys665-Trp666, assume dihedral angles compatible with a canonical α -helix (Figure 7A). These crystals were obtained from a solution containing sulfate in the mother liquor. In contrast, 2F5 Fab'-scrHybK3 cocrystal diffraction data did not produce interpretable electron density for residues Ser668-Leu669-Trp670-Asn671 (crystals obtained from a solution without sulfate, Figure 7B) and for residues Leu669-Trp670-Asn671 (crystals soaked in a solution containing sulfate, Figure 7C). From the comparison of these structures, it can be inferred that the correct FP sequence caused the creation of a carboxy-terminal α -helix following the core type I β -turn in the gp41 native structure recognized by the 2F5 antibody.

As shown in Table 4, the presence of the carboxy-terminal helix also correlated with a significant increase in the surface area of the peptide epitope that is buried in the interaction with 2F5 Fab' (from 344.4 to 554.1 Å²). Accordingly, the buried

surface areas of the Fab' light and heavy chains were also larger in the interaction with HybK3. Thus, it seems that FP residues induce structural constraints that result in the establishment of more efficient interactions with 2F5 Fab'.

Discussion

Antibodies raised to recapitulate the 2F5-binding mechanism are assumed to exert a qualitatively similar neutralizing activity. Consequently, several attempts have been made to produce peptide-based formulations capable of inducing 2F5-like immune responses.^{12,13} Conformationally constrained cyclic peptides designed to adopt β -turns showed increased MAbs2F5 affinity.^{39,40} 2F5ep-like elongated linear epitopes also showed higher Mab2F5 affinity when compared to the ELDKWA core.^{39,41–44} However, these peptide-based vaccines elicited antipeptide antibodies that were non-neutralizing. Thus, the failures in recovering NAb-s after immunization suggest that the 2F5 antigenic determinant in the native gp41 ectodomain is probably more structurally complex than that represented by the linear epitope.^{17,45}

Structural studies actually support the intrinsic flexibility of the elongated 2F5 epitope sequence in isolation.^{17,18,39,41,42,46–48} Thus, peptides encompassing the full epitope exhibited in solution several conformations, which mostly included for this stretch a combination of turns and 3₁₀-helices with unordered structures.^{17,18,42,46–48} Interestingly, access to these different conformations was unaffected by temperature in the 1–60 °C interval.⁴⁶ The absence of a single, favored conformation in the linear sequence implies that, on the native antigen, the 2F5 epitope must be by unknown mechanisms constrained into the distinct MPER structure recognized by the antibody.¹⁵

In previous work, we proposed that contacts with amino-terminal FP residues might contribute to the stabilization of the gp41 native structure recognized by MAbs2F5.^{17,18} Recent mutational and structural studies support the establishment of functional contacts between N- and C-terminal ectodomain sequences at the various stages of the gp41-induced fusion cycle.^{49,50} Cryoelectron tomography of viral spikes reported by Roux and co-workers^{51,52} was consistent with the MPER region being already in contact with the membrane interface in native prefusion Env. This observation puts forward the possibility that FP-MPER contacts might be affected by the reduction in medium polarity sensed in the vicinity of the lipid bilayer.²⁹ Notably, the native structure recognized by MAbs2F5 appears to depend also on temperature-modulated elements. Early observations indicated that MAbs2F5 did not react with Env-expressing or virus-infected cells at 4 °C.^{20,21} Finnegan and co-workers characterized further the temperature dependence of binding and found a threshold temperature, 19 °C, below which mAb reactivity was not detectable.²¹ This phenomenon was demonstrated not to involve temperature-induced shedding of the surface gp120 subunit. Thus, these authors concluded that 2F5 epitope exposure above 19 °C might reflect either an increase of spike flexibility and/or the existence of unknown, temperature-dependent conformational elements on the prefusion native antigen.

The structural characterization described here is further consistent with the idea that FP interactions might stabilize MPER native-like structures in close proximity to the membrane interface (Figure 2 and Table 1). In addition to the reduction in medium polarity, we observed that the structural constraints imposed by the FP residues may vary with temperature (survey displayed in Figure 8A and Table 2). Conformations described to be equally accessible to the 2F5ep sequence in isolation,⁴⁶

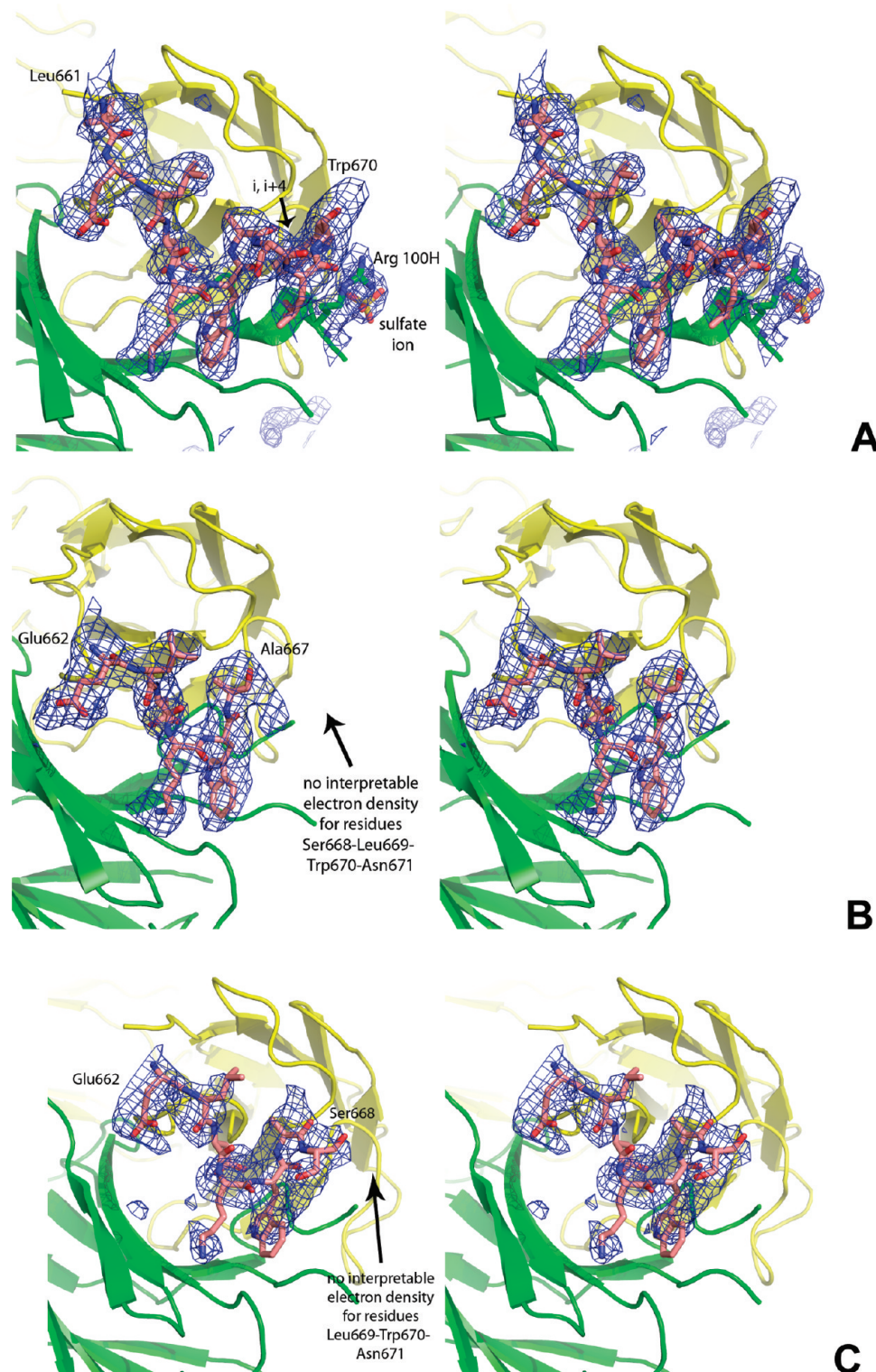


Figure 7. Stereoviews of the crystal structures of 2F5 Fab' in complex with different constructs. (A) Crystal structure of the 2F5 Fab' cocrystallized with peptide Hyb3K, grown in a solution containing 1.6 M ammonium sulfate (PDB ID: 3D0L). (B) Crystal structure of 2F5 Fab' cocrystallized with peptide scrHyb3K, grown without sulfate (16% PEG 4000 and 16% 2-propanol) (PDB ID: 3DRT). (C) Crystal structure of 2F5 Fab' cocrystallized with peptide scrHyb3K, and subsequently transferred into a solution containing 1.6 M ammonium sulfate (PDB ID: 3EGS). This procedure generated an environment comparable to the one for 2F5 Fab'-Hyb3K crystals, especially providing sulfate ions. The gp41 epitope residues for which electron density is observed are shown as a salmon-colored stick model. The 2F5 Fab' is rendered as a cartoon model according to its secondary structure, with the heavy chain in green and the light chain in yellow. Electron density is shown in blue as an $F_o - F_c$ simulated annealing omit map with a 2.0σ contour level. To allow for easier comparison, all electron density maps were calculated at a resolution of 3.6 \AA .

i.e., 3_{10} -helices (**) and β -turns (*) were alternatively favored below and above 20°C in the HybK3 peptide (Figures 3–6). Furthermore, the 2D-COS IR analysis indicated that the β -turns

accumulating above ca. 20°C arise from the 3_{10} -helix structures existing below this temperature (Figures 4 and 5). Thus, our data suggest that temperature might drive the conversion of the

TABLE 3: Statistics for 2F5 Fab'-scrHybK3 Complex X-ray Data Collection and Model Refinement^a

crystal data	2F5 Fab'-scrHyb3K	2F5 Fab'-scrHyb3K
crystal growth	16% PEG 4K, 16% 2-propanol	16% PEG 4K, 16% 2-propanol soak: 1.6 M ammonium sulfate
PDB ID	3DRT	3EGS
space group	P2 ₁ 2 ₁ 2 ₁	P2 ₁ 2 ₁ 2 ₁
unit cell axes (Å)	<i>a</i> = 64.2 <i>b</i> = 76.4 <i>c</i> = 93.6	<i>a</i> = 63.8 <i>b</i> = 75.9 <i>c</i> = 93.5
resolution range (Å)	17.0–3.3 (3.51–3.3)	17.0–3.6 (3.65–3.60)
$\langle I \rangle / \langle \sigma(I) \rangle$	8.1 (4.2)	4.7 (3.0)
completeness (%)	94.0 (89.6)	95.5 (99.5)
measured reflections	61120	21508
unique reflections	6826	5386
R_{sym} (%)	26.5 (49.7)	28.0 (46.2)
Refinement		
resolution (Å)	17.0–3.3	17.0–3.60
number of protein atoms/solvent molecules	3316/0	3321/0
rmsd bond length (Å)/angles (deg)	0.009/1.8	0.008/1.8
number of reflections $R_{\text{work}}/R_{\text{free}}$	6480/346	4828/240
Ramachandran: preferred region/outliers (%)	89.7/2.8	92.5/1.6
$R_{\text{cryst}}/R_{\text{free}}$ (%)	20.3/22.9	23.5/24.9
average overall <i>B</i> value (Å ²)	19.0	23.5

^a Values in parentheses represent those in the highest resolution bin.

TABLE 4: Contact Surface Areas by Residue on Peptide Epitopes and 2F5 Fab'

peptide residue	contact area (Å ²)	Fab' residue, light chain	contact area (Å ²)	Fab' residue, heavy chain	contact area (Å ²)
2F5 Fab'-HybK3 Structure (3D0L)					
Leu661	75.9	Tyr94	74.9	Arg100H	70.1
Glu662	57	Phe93	53.2	Pro98	34.3
Leu663	41.2	His92	45.4	Val100K	28
Asp664	72.9	Leu2	13.8	Arg95	25.7
Lys665	75	Gln27	13.7	Tyr52	25.4
Trp666	93.8	Leu91	11.3	Arg58	17.5
Ala667	15.1	His96	8.7	Gly33	15.4
Ser668	0	Ala1	7.5	Asp56	15.2
Leu669	42	Pro95	5.7	Asp54	13.8
Trp670	81.2	Ser31	4.2	Asn100L	12.6
total:	554.1	Asp50	2.2	Phe32	9.7
		total:	240.6	Gly100I	7.7
				Gly97	1.6
				total:	277
2F5 Fab'-scrHybK3 Structure (3EGS)					
Glu662	54.7	Tyr94	56	Pro98	27.4
Leu663	39.6	His92	45.1	Arg95	24.3
Asp664	70.5	Phe93	35.5	Val100K	21.4
Lys665	64.6	Leu91	10.3	Tyr52	19
Trp666	101.8	His96	7.5	Arg58	17.7
Ala667	13.2	total:	154.4	Asp56	13.4
Ser668	0			Asp54	13
total:	344.4			Gly33	11.8
				Phe32	10
				Gly97	1.6
				total:	159.6

FP-constrained 2F5ep structure into a main conformation physiologically relevant for MAb2F5 binding,¹⁶ and that this conversion would be essentially reversible (Figure 6). Immersion into a low polarity medium abolishes this conversion, and favors the helical conformations. The relevance of the FP sequence in these processes is supported by the data obtained using the scrHybK3 variant. Scrambling the conserved FP residues reduced the helical content (Figure 2 and Table 1) and abolished the thermal transition (Figures 3 and 4). In line with these observations, the crystallographic results suggest that the FP residues in the correct order influence the formation of a canonical α -helix by the sequence C-terminally flanking the 2F5

DKW core epitope (Figure 7). Additionally, the presence of the helix results in a more efficient Fab'-peptide interaction (Table 4).

The model depicted in Figure 8B illustrates the fact that within the MPER stretch of the HybK3 structure the helix main axis forms an almost square angle with the amino-terminal extended chain. Thus, the HybK3 structure further suggests an unforeseen function for the type I β -turn element as a molecular hinge that induces a 90° directional change in the MPER chain path (Figure 7A and ref 16). The model also suggests that low temperature and/or polarity might induce the adoption of a rigid 3₁₀-helical structure by the LLELDKW as proposed by Biron

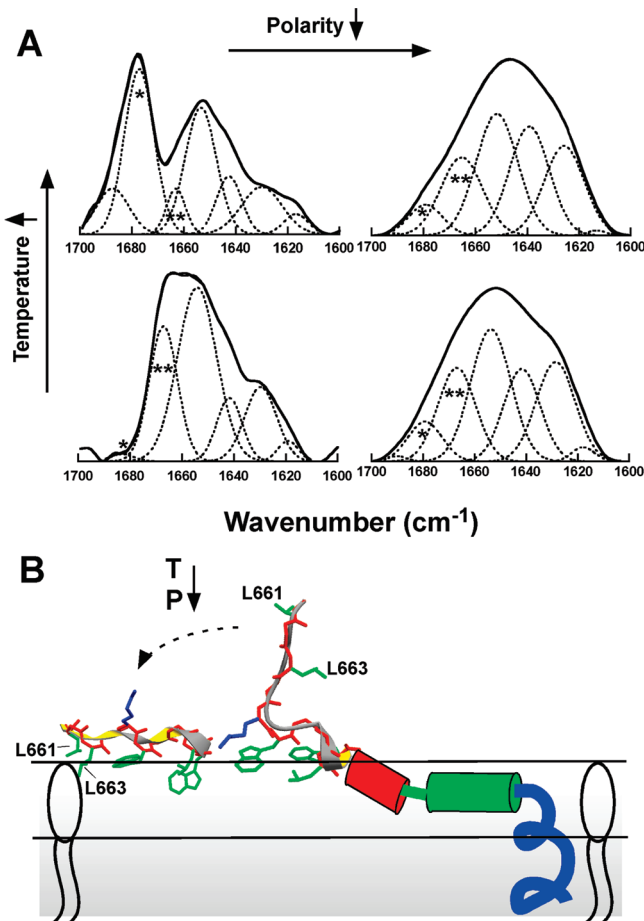


Figure 8. (A) Survey of IR results: HybK3 amide I structural components in 5 and 50% HFIP (left and right panels, respectively) are compared. Top and bottom panels correspond to spectra obtained at 50 and 4 °C, respectively. The numerical values are presented in Table 2. (B) Hypothetical model to explain temperature and polarity effects on the 2F5 epitope MPER region. The turn-hinge structure recognized by the antibody (right) would disrupt the membrane-inserted amphipathic-at-interface α -helix^{18,54} (red cylinder) and induce a change in gp41 chain path orientation. Reduction in temperature and/or polarity might induce the refolding of the turn and the preceding extended stretch into a more rigid 3_{10} -helix,⁴⁸ which might associate with the membrane interface (left). Hydrophobic-at-interface residues²⁹ are designated by the green side-chains. The blue side-chain designates Lys665.

et al.⁴⁸ This transition would redirect the gp41 main chain, which would advance in parallel to the membrane plane, and project the hydrophobic-at-interface residues toward the membrane interface (left). At the physiological temperature, FP interactions might stabilize the turn-hinge structure orienting the gp41 chain perpendicular to the membrane plane (right). The neutralizing 2F5 mAb seems to be adapted for the recognition of this structural motif in the membrane context.^{12,13,15,16,53} Thus, the proposed model underlines the importance of the membrane–water interface in the stabilization and folding of the membrane-proximal gp41 ectodomain regions.²⁹ Moreover, the model supports the importance of recreating FP-induced interactions and structures in effective synthetic AIDS vaccines targeted to the MPER region.

Acknowledgment. This study was supported by Spanish MICINN (BIO2008-00772 to J.L.N. and BFU2006-14423 to J.L.R.A.) and the University of the Basque Country (GIU 06/42 and DIPE08/12) (J.L.N. and J.L.R.A.), as well as by a University of Toronto Research Program grant sponsored by

Sanofi-Pasteur Canada, the Canada Research Chairs Program (E.F.P.) and a CIHR pre-doctoral fellowship (J.-P.J.).

References and Notes

- Burton, D. R.; Desrosiers, R. C.; Doms, R. W.; Koff, W. C.; Kwong, P. D.; Moore, J. P.; Nabel, G. J.; Sodroski, J.; Wilson, I. A.; Wyatt, R. T. *Nat. Immunol.* **2004**, 5, 233.
- Walker, B. D.; Burton, D. R. *Science* **2008**, 320, 760.
- Thayer, A. *Chem. Eng. News* **2008**, 86, 17.
- Karlsson Hedestam, G. B.; Fouchier, R. A.; Phogat, S.; Burton, D. R.; Sodroski, J.; Wyatt, R. T. *Nat. Rev. Microbiol.* **2008**, 6, 143.
- Douek, D. C.; Kwong, P. D.; Nabel, G. J. *Cell* **2006**, 124, 677.
- Burton, D. R. *Nat. Rev. Immunol.* **2002**, 2, 706.
- Binley, J. M.; Wrin, T.; Korber, B.; Zwick, M. B.; Wang, M.; Chappay, C.; Stiegler, G.; Kunert, R.; Zolla-Pazner, S.; Katinger, H.; Petropoulos, C. J.; Burton, D. R. *J. Virol.* **2004**, 78, 13232.
- Muster, T.; Guineo, R.; Trkola, A.; Purtscher, M.; Klima, A.; Steindl, F.; Palese, P.; Katinger, H. *J. Virol.* **1994**, 68, 4031.
- Frankel, S. S.; Steinman, R. M.; Michael, N. L.; Kim, S. R.; Bhardwaj, N.; Pope, M.; Louder, M. K.; Ehrenberg, P. K.; Parren, P. W.; Burton, D. R.; Katinger, H.; VanCott, T. C.; Robb, M. L.; Birx, D. L.; Mascola, J. R. *J. Virol.* **1998**, 72, 9788.
- Mascola, J. R.; Stiegler, G.; VanCott, T. C.; Katinger, H.; Carpenter, C. B.; Hanson, C. E.; Beary, H.; Hayes, D.; Frankel, S. S.; Birx, D. L.; Lewis, M. G. *Nat. Med.* **2000**, 6, 207.
- Ferrantelli, F.; Hofmann-Lehmann, R.; Rasmussen, R. A.; Wang, T.; Xu, W.; Li, P. L.; Montefiori, D. C.; Cavacini, L. A.; Katinger, H.; Stiegler, G.; Anderson, D. C.; McClure, H. M.; Ruprecht, R. M. *AIDS* **2003**, 17, 301.
- Zwick, M. B. *AIDS* **2005**, 19, 1725.
- Montero, M.; van Houten, N. E.; Wang, X.; Scott, J. K. *Microbiol. Mol. Biol. Rev.* **2008**, 72, 54.
- Pai, E.; Klein, M.; Chong, P.; Pedy-czak, A. Fab-epitope complex from the HIV-1 cross-neutralizing monoclonal antibody 2F5. In World Intellectual Property Organization 2000; Vol. patent WO-00/61618.
- Ofek, G.; Tang, M.; Sambor, A.; Katinger, H.; Mascola, J. R.; Wyatt, R.; Kwong, P. D. *J. Virol.* **2004**, 78, 10724.
- Julien, J. P.; Bryson, S.; Nieva, J. L.; Pai, E. F. *J. Mol. Biol.* **2008**, 384, 377.
- Lorizate, M.; Gomara, M. J.; de la Torre, B. G.; Andreu, D.; Nieva, J. L. *J. Mol. Biol.* **2006**, 360, 45.
- Lorizate, M.; de la Arada, J.; Huarte, N.; Sanchez-Martinez, S.; de la Torre, B. G.; Andreu, D.; Arrondo, J. L.; Nieva, J. L. *Biochemistry* **2006**, 45, 14337.
- Lorizate, M.; Huarte, N.; Saez-Cirion, A.; Nieva, J. L. *Biochim. Biophys. Acta* **2008**.
- Sattentau, Q. J.; Zolla-Pazner, S.; Poignard, P. *Virology* **1995**, 206, 713.
- Finnegan, C. M.; Berg, W.; Lewis, G. K.; DeVico, A. L. *J. Virol.* **2002**, 76, 12123.
- Bryson, S.; Cunningham, A.; Ho, J.; Hynes, R. C.; Isenman, D. E.; Barber, B. H.; Kunert, R.; Katinger, H.; Klein, M.; Pai, E. F. *Protein Pept. Lett.* **2001**, 8, 413.
- Arrondo, J. L.; Goni, F. M. *Prog. Biophys. Mol. Biol.* **1999**, 72, 367.
- Iloro, I.; Chehin, R.; Goni, F. M.; Pajares, M. A.; Arrondo, J. L. *Biophys. J.* **2004**, 86, 3951.
- Kabsch, W. J. *J. Appl. Crystallogr.* **1993**, 26, 795.
- Brunger, A. T.; Adams, P. D.; Clore, G. M.; DeLano, W. L.; Gros, P.; Grosse-Kunstleve, R. W.; Jiang, J. S.; Kuszewski, J.; Nilges, M.; Pannu, N. S.; Read, R. J.; Rice, L. M.; Simonson, T.; Warren, G. L. *Acta Crystallogr., Sect. D* **1998**, 54, 905.
- Emsley, P.; Cowtan, K. *Acta Crystallogr., Sect. D* **2004**, 60, 2126.
- Cardozo, T.; Totrov, M.; Abagyan, R. *Proteins* **1995**, 23, 403.
- White, S. H.; Wimley, W. C. *Annu. Rev. Biophys. Biomol. Struct.* **1999**, 28, 319.
- Gallagher, W. R. *Cell* **1987**, 50, 327.
- Seerama, N.; Woody, R. W. *Methods Enzymol.* **2004**, 383, 318.
- Arrondo, J. L.; Muga, A.; Castresana, J.; Goni, F. M. *Prog. Biophys. Mol. Biol.* **1993**, 59, 23.
- Perczel, A.; Fasman, G. D. *Protein Sci.* **1992**, 1, 378.
- Keating, A. E.; Malashkevich, V. N.; Tidor, B.; Kim, P. S. *Proc. Natl. Acad. Sci. U.S.A.* **2001**, 98, 14825.
- Litowski, J. R.; Hodges, R. S. *J. Biol. Chem.* **2002**, 277, 37272.
- Fabian, H.; Mantsch, H. H.; Schultz, C. P. *Proc. Natl. Acad. Sci. U.S.A.* **1999**, 96, 13153.
- Noda, I. *Anal. Sci.* **2007**, 23, 139.
- Arrondo, J. L.; Blanco, F. J.; Serrano, L.; Goni, F. M. *FEBS Lett.* **1996**, 384, 35.
- Tian, Y.; Ramesh, C. V.; Ma, X.; Naqvi, S.; Patel, T.; Cenizal, T.; Tiscione, M.; Diaz, K.; Crea, T.; Arnold, E.; Arnold, G. F.; Taylor, J. W. *J. Pept. Res.* **2002**, 59, 264.

- (40) McGaughey, G. B.; Citron, M.; Danzeisen, R. C.; Freidinger, R. M.; Garsky, V. M.; Hurni, W. M.; Joyce, J. G.; Liang, X.; Miller, M.; Shiver, J.; Bogusky, M. J. *Biochemistry* **2003**, *42*, 3214.
- (41) Joyce, J. G.; Hurni, W. M.; Bogusky, M. J.; Garsky, V. M.; Liang, X.; Citron, M. P.; Danzeisen, R. C.; Miller, M. D.; Shiver, J. W.; Keller, P. M. *J. Biol. Chem.* **2002**, *277*, 45811.
- (42) Barbato, G.; Bianchi, E.; Ingallinella, P.; Hurni, W. H.; Miller, M. D.; Ciliberto, G.; Cortese, R.; Bazzo, R.; Shiver, J. W.; Pessi, A. *J. Mol. Biol.* **2003**, *330*, 1101.
- (43) Parker, C. E.; Deterding, L. J.; Hager-Braun, C.; Binley, J. M.; Schulke, N.; Katinger, H.; Moore, J. P.; Tomer, K. B. *J. Virol.* **2001**, *75*, 10906.
- (44) Sanchez-Martinez, S.; Lorizate, M.; Hermann, K.; Kunert, R.; Basanez, G.; Nieva, J. L. *FEBS Lett.* **2006**, *580*, 2395.
- (45) Menendez, A.; Chow, K. C.; Pan, O. C.; Scott, J. K. *J. Mol. Biol.* **2004**, *338*, 311.
- (46) Ahmed, Z.; Asher, S. A. *Biochemistry* **2006**, *45*, 9068.
- (47) Biron, Z.; Khare, S.; Quadt, S. R.; Hayek, Y.; Naider, F.; Anglister, J. *Biochemistry* **2005**, *44*, 13602.
- (48) Biron, Z.; Khare, S.; Samson, A. O.; Hayek, Y.; Naider, F.; Anglister, J. *Biochemistry* **2002**, *41*, 12687.
- (49) Bellamy-McIntyre, A. K.; Lay, C. S.; Baar, S.; Maerz, A. L.; Talbo, G. H.; Drummer, H. E.; Poumbourios, P. *J. Biol. Chem.* **2007**, *282*, 23104.
- (50) Noah, E.; Biron, Z.; Naider, F.; Arshava, B.; Anglister, J. *Biochemistry* **2008**, *47*, 6782.
- (51) Roux, K. H.; Taylor, K. A. *Curr. Opin. Struct. Biol.* **2007**, *17*, 244.
- (52) Zhu, P.; Liu, J.; Bess, J., Jr.; Chertova, E.; Lifson, J. D.; Grise, H.; Ofek, G. A.; Taylor, K. A.; Roux, K. H. *Nature* **2006**, *441*, 847.
- (53) Sanchez-Martinez, S.; Lorizate, M.; Katinger, H.; Kunert, R.; Nieva, J. L. *AIDS Res. Hum. Retroviruses* **2006**, *22*, 998.
- (54) Sun, Z. Y.; Oh, K. J.; Kim, M.; Yu, J.; Brusic, V.; Song, L.; Qiao, Z.; Wang, J. H.; Wagner, G.; Reinherz, E. L. *Immunity* **2008**, *28*, 52.

JP905965H